Scripta Materialia 198 (2021) 113838

Contents lists available at ScienceDirect

Scripta Materialia

journal homepage: www.elsevier.com/locate/scriptamat

Improving creep resistance of Al-12 wt.% Ce alloy by microalloying with Sc

Meng Yi[a], Peng Zhang[a,*], Chong Yang[a], Pengming Cheng[a], Shengwu Guo[a], Gang Liu[a,*], Jun Sun[a,*]

State Key Laboratory for Mechanical Behavior of Materials, Xi'an Jiaotong University, Xi'an, 710049, China

ARTICLE INFO

Article history:
Received 28 December 2020
Revised 23 February 2021
Accepted 1 March 2021

Keywords:
Al-Ce alloy
Eutectic
Al_3Sc
Creep

ABSTRACT

The near-eutectic Al-12 wt.% Ce alloy has been alloyed with 0.4 wt.% Sc to improve its creep resistance. A bidirectional influence between Sc and Ce has been identified: (i) the Ce element suppresses the Sc partition between the liquid and solid phases during solidification, as implied by the reduction of Sc microsegregation in the as-cast ingot; (ii) the Sc atoms migrate towards the $Al_{11}Ce_3$ interface to form Al_3Sc thin layer or particles upon aging. The former effect promotes the spatial uniformity of Al_3Sc precipitate distribution in the Al matrix and the latter one introduces additional lattice misfit strain to the $Al_{11}Ce_3/Al_\alpha$ phase boundary inhibiting matrix dislocations to climb over the $Al_{11}Ce_3$ lamellae. Both effects can improve the creep resistance of the aged Al-12Ce-0.4Sc alloy showing a high tensile stress threshold for dislocation creep of ~ 60 MPa at 300 °C.

Aluminum alloys have been widely used as lightweight structural materials at *ambient* temperature [1–4]. However, expanding their applications to *elevated* temperature faces great challenges for the rapid coarsening or dissolution of nanosized second phase(s) degenerating mechanical properties [5]. As a consequence, most of them, including the Al-Si(-Cu)- and Al-Cu-Mg-based alloys having gained a certain market share in automobile engines, are limited to temperatures below 250 °C [6,7]. To forward Al alloys towards higher temperature, a highly thermally stable microstructure is desirable.

Recently, the Al alloys with a high content of cerium, a relatively low-priced and abundant by-product of rare-earth mining, have been attracting increasing attention [8–13]. The Al-Ce alloy with the eutectic composition (~ 10 wt.%) is compatible with modern casting practices due to its exceptional castability even exceeding the Al-Si system [14]. The cast eutectic Al-Ce alloy consists of highly branched submicron-sized $Al_{11}Ce_3$ lamellae surrounded by almost pure Al [8]. This microstructure is extremely stable against the long-time heat-exposure up to 400 °C or higher [8,15] because the coarsening is hard to proceed when the diffusion of Ce atoms between the neighboring $Al_{11}Ce_3$ lamellae is almost forbidden by the negligible solid solubility of Ce in Al ($\leq$ 0.005 wt.% at 642 °C [8]) and the low diffusivity of Ce in Al, estimated as $\sim 4.7 \times 10^{-19}$ s^{-1} at 400 °C, much smaller than that of Si, Cu or Sc by more than one order of magnitude [15]. Consequently, the Al-Ce alloy holds an outstanding retention of strength at elevated temperatures [8,15]. Besides, appropriate alloying the Al-Ce alloy with, for instance, Mg and Si [10,13], can provide the additional solid-solution and precipitation strengthening improving further its mechanical properties.

To date, the studies of mechanical properties of Al-Ce-based alloys have mostly focused on the strength and ductility under quasi-static tensile loading conditions [8–10,12,14,16]. However, for the materials in high-temperature service, the creep strain accumulating over a long-term heat-exposure can be prominent and ultimately results in failure of component under a stress below yield strength. Nonetheless, only recently, the creep behaviors were studied in an Al-12.5 wt.%Ce alloy [15] and an Al-6.9 wt.%Ce-9.3 wt.%Mg alloy [13]. The stress threshold of dislocation creep was measured to be ~ 22 MPa at 300 °C for the former alloy, superior to the latter one containing fast-creeping Al-Mg matrix, but inferior to, for instance, the newly developed Al alloys containing coarsening-resistant plate-like precipitates [17,18]. To improve the creep resistance of Al-Ce alloy, in this study, we alloyed it with Sc to form thermally stable Al_3Sc coherent precipitates [19], which can inhibit the dislocation climb effectively due to the misfit strain around the precipitates [20–22]. The same methodology of combining the advantages of eutectic and coherent nano-particles has been utilized in, for instance, Refs[23–26]. In particular, an outstanding creep resistance has been achieved in a eutectic Al-Ni al-

* Corresponding authors.
E-mail addresses: zhangpeng.mse@xjtu.edu.cn (P. Zhang), lgsammer@xjtu.edu.cn (G. Liu), junsun@xjtu.edu.cn (J. Sun).

https://doi.org/10.1016/j.scriptamat.2021.113838
1359-6462/

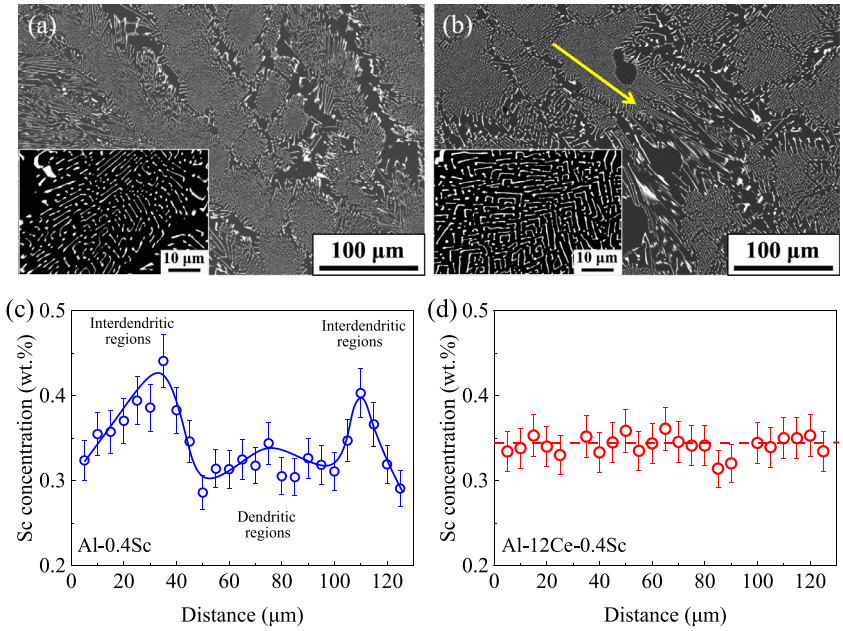

Fig. 1. Characterization of eutectic structure and Sc distribution in the as-cast alloy. **(a)** and **(b)** Characteristic SEM images of the Al-12Ce and Al-12Ce-0.4Sc alloys, with insets showing the structure within the eutectic colony. **(c)** and **(d)** EPMA line profile of Sc concentration for the as-cast Al-0.4Sc and Al-12Ce-0.4Sc alloys, respectively.

loy with Sc addition [23]. However, the effectiveness of Sc addition in the Al-Ce system and the associated origin of enhanced creep properties, which should be of value for further developments of Al-Ce-Sc-based alloys, have not been investigated.

The Al-12 wt.% Ce (Al-12Ce), Al-0.4 wt.% Sc (Al-0.4Sc), and Al-12 wt.% Ce-0.4 wt.% Sc (Al-12Ce-0.4Sc) alloys were respectively melted under the argon protection and then cast into a steel mold preheated to 200 °C. The distribution of Sc in the as-cast ingot was examined using electron probe micro-analysis (EPMA), based on which the aging procedure was decided. The alloy microstructure was characterized using scanning electron microscopy (SEM), transmission electron microscopy (TEM), and high-resolution TEM (HRTEM). Samples for tensile creep experiments were machined from the center of the ingot and tested in the atmosphere under a constant load at 300 °C. When the steady-state creep deformation was achieved, the load was increased to a value corresponding to a 2.5 MPa ∼ 5 MPa increment of engineering stress.

The eutectic structure of the as-cast Al-12Ce alloy is shown in Fig. 1(a). It comprises $Al_{11}Ce_3/Al_\alpha$ eutectic colonies separated by pure Al channels or by channels with large and sparsely distributed $Al_{11}Ce_3$ intermetallic. In the eutectic colony, the fine $Al_{11}Ce_3$ platelets with a width of 150 nm ∼ 450 nm arrange into a labyrinth-like morphology (inset of Fig. 1(a)). The average aisle width of "labyrinth" (i.e., eutectic spacing) was measured to be 1.71 ± 0.23 μm. With 0.4 wt.% Sc addition there is no identifiable change for the eutectic morphology and the structure in between the eutectic colonies (see Fig. 1(b)), except that the eutectic spacing was measured as 2.18 ± 0.97 μm, slightly larger than, but not significantly different from, that of the Al-Ce binary alloy, indicating that the Sc has a minor influence on the solidification of Al-Ce liquid.

On the other hand, the abundant Ce atoms significantly optimize the Sc atom distribution in the Al-12Ce-0.4Sc alloy after solidification. To demonstrate this point convincingly, it is necessary to compare the distribution of Sc between the alloys with and without Ce. Based on this consideration, we first show the Sc distribution for the as-cast Al-0.4Sc alloy in Fig. 1(c), where the EPMA line profile reveals a periodic fluctuation of Sc concentration within a wide range of 0.28 wt.% ∼ 0.44 wt.%. This is because Sc forms a terminal eutectic with Al, with an equilibrium solid-liquid partition coefficient k_0 smaller than one [27,28]. In this case, the first solid forming during solidification contains less Sc than the solid to form later, leading to the non-uniform Sc distribution at the dendritic scale. However, this harmful Sc microsegregation in Al_α largely disappears for the Al-12Ce-0.4Sc alloy, as suggested by the smooth EPMA line profile of Sc concentration in Fig. 1(d). It is common that the equilibrium partition coefficient k_0 changes for the addition of other elements since the partition behavior strongly correlates with element interactions [29]. In this sense, the suppression of Sc microsegregation in the Al-12Ce-0.4Sc alloy implies that the Ce element increases k_0 of Sc towards one, and thus minimizing the Sc partition between the liquid and solid phases during solidification [30].

This resultant uniformity of Sc distribution is highly desirable, as it avoids the homogenization treatment that would be performed around 640 °C to eliminate the Sc microsegregation [20,31]. Note that the heat-treatment at such a high temperature remains a challenge for the casting alloy as it may induce severe distortion and residual stress to casting components complex in shape [32]. Therefore, we passed the homogenization treatment and directly aged the Al-12Ce-0.4Sc alloy at relatively low temperatures (first at 300 °C for 5 h and then at 400 °C for 1 h, 3 h or 8 h) to precipitate Al_3Sc particles.

Due to the suppression of Sc partition in the Al-12Ce-0.4Sc alloys, we found that, upon aging, the number density and average size of Al_3Sc precipitates are almost the same at different positions we measured within the Al_α eutectic, see Fig. 2(a) and (b). Moreover, dense Al_3Sc precipitates with a similar number density were also observed in the channels between the eutectic colonies. In contrast, the Sc concentration fluctuation in the as-cast Al-0.4Sc alloy results in an aged microstructure with alternative Al_3Sc-depleted (Fig. 1(c)) and Al_3Sc-enriched (Fig. 1(d)) regions corresponding to the dendritic and interdendritic areas respectively. The fast creep of the precipitate-depleted regions is deleterious for the high-temperature performance [33]. Thereby, we can say that the Sc addition can suppress the creep of Al_α in the Al-12Ce-0.4Sc alloy effectively, especially considering its absence of precipitate-depleted regions. Moreover, this effective en-

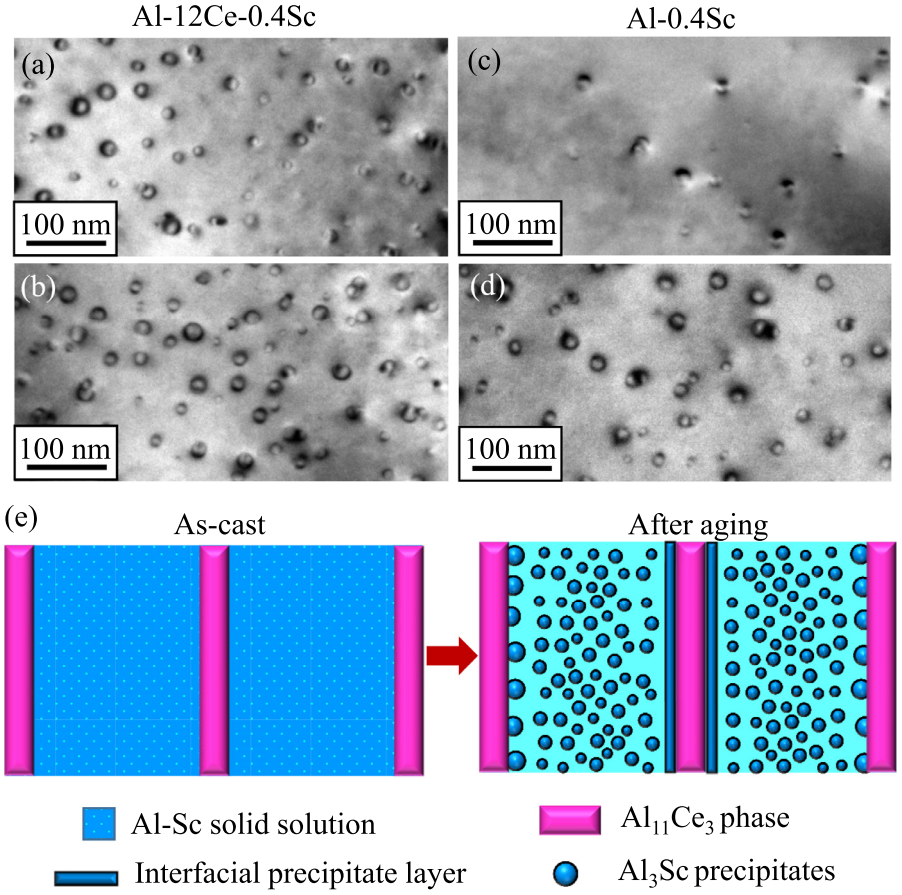

Fig. 2. Characterization of Al_3Sc precipitates. **(a)** and **(b)** Bright field TEM images taken at different positions of the Al-12Ce-0.4Sc alloy aged at 300 °C for 5 h and then at 400 °C for 3 h. **(c)** and **(d)** Bright field TEM images taken at different positions of the Al-0.4Sc alloy with the same aging treatment as the Al-12Ce-0.4Sc alloy in (a) and (b). **(e)** Sketch showing the Al_3Sc precipitation in the Al-12Ce-0.4Sc alloy.

hancement of Al_α phase can promote the load transfer from the soft Al_α phase to the hard $Al_{11}Ce_3$ intermetallic [8], thus improving further the creep resistance of the Al-12Ce-0.4Sc alloy.

Besides the Al_3Sc precipitates in the Al matrix, the $Al_{11}Ce_3/Al_\alpha$ interface should be also paid attention to, as the $Al_{11}Ce_3$-dislocation interaction associated with the interfacial structure has been argued as another main mechanism determining the elevated-temperature strength of Al-Ce alloy [15]. A previous study revealed in an Al-Ce-Mg alloy that the Al_α and $Al_{11}Ce_3$ phases hold a coherent relation [8]; however, we checked more than ten cases of $Al_{11}Ce_3/Al_\alpha$ interfaces in the Al-Ce alloy, without encountering a coherent alignment, indicating that the coherent relation is rare in, at least, the binary Al-Ce alloy. Fig. 3(a) gives a typical example of our observation, where the Al_α phase aligns along its $[100]_{Al}$ zone axis, while the $Al_{11}Ce_3$ phase still deviates from its zone axis and its lattice is not very clear. By tilting ~ 6° away from the $[100]_{Al}$ zone axis, the $[111]_{Al_{11}Ce_3}$ zone axis was reached. With such a large misalignment, the coherency is largely lost (Fig. 3(a)), and the $Al_{11}Ce_3/Al_\alpha$ interface should be more close to incoherent than coherent.

Actually, our result is fully consistent with a recent TEM investigation revealing that the coherent relation holds only at the initial stage of nucleation and growth of $Al_{11}Ce_3$ lamella during solidification [34]. As the growth of $Al_{11}Ce_3$ proceeds, the two eutectic phases tilt away from their initial orientation relation for several degrees to release the misfit strain; correspondingly, the $Al_{11}Ce_3/Al_\alpha$ interfacial relation evolves from coherent to semi-coherent and then to *incoherent* after solidification [34].

For the Al-12Ce-0.4Sc alloy, the modification of $Al_{11}Ce_3/Al_\alpha$ interface occurs upon aging, which should impact its high-temperature mechanical properties considering that its interface area to volume ratio is significant. Fig. 3(b) is a representative bright-field TEM image of the aged Al-12Ce-0.4Sc alloy, where the precipitate-free zones (PFZs) with a width of ~ 100 nm appear nearby the $Al_{11}Ce_3$ lamella. Similar PFZs nearby the θ'-Al_2Cu precipitates have also been observed in an aged Al-Cu-Sc alloy [17], with Al_3Sc particles precipitating on the θ'-Al_2Cu/Al_α interface. Similarly, we found in our aged Al-12Ce-0.4Sc alloy that the Sc atoms within the PFZs have migrated to the $Al_{11}Ce_3/Al_\alpha$ interface and formed interfacial Al_3Sc precipitates.

Two types of interfacial Al_3Sc precipitates varying in morphology have been identified: (i) a thin layer of Al_3Sc precipitation, as indicated in the dark-field image taken using (100) diffraction spot associated with the Al_3Sc precipitates in Fig. 3(c); and (ii) spherical Al_3Sc particles, as shown by the bright field image in Fig. 3(d) and the corresponding energy dispersive spectrometer (EDS) Sc mapping in Fig. 3(e). The Al_3Sc morphology may be determined by the orientation relationship between the $Al_{11}Ce_3$ and Al_α phases. However, the key point we focus on is that the interfacial Al_3Sc precipitates, regardless of their morphology, are coherent with the Al_α matrix, see Fig. 3(f), and thus introducing substantial misfit strain to the $Al_{11}Ce_3/Al_\alpha$ interface that was more likely to be semi-coherent or incoherent. It has been known, from the theory [35,36] and experiments [5,22], that the threshold stress σ_{th} below which the dislocations are unable to climb over the precipitates is determined by the magnitude of lattice mismatch strain around precipitates. Therefore, generating (or enhancing) the misfit strain

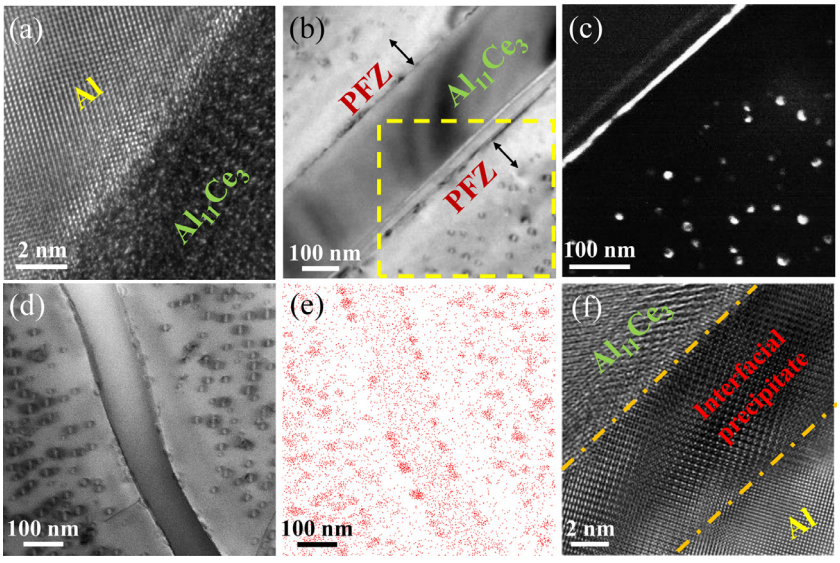

Fig. 3. Characterization of $Al_{11}Ce_3/Al_\alpha$ interfacial structure. **(a)** Interfacial atomic structure in the as-cast Al-12Ce alloy. **(b)** Bright-field image of the Al-12Ce-0.4Sc alloy aged at 300 °C for 5 h and then at 400 °C for 3 h. **(c)** Dark-field image of (100) diffraction spot for the marked area in (b). **(d)** shows the precipitation of sphere Al_3Sc particles at interface in the same material of (b). **(e)** EDS mapping of Sc element corresponding to (d). **(f)** HRTEM image of the $Al_{11}Ce_3/Al_3Sc/Al_\alpha$ interface.

on the boundary of $Al_{11}Ce_3$ and Al_α should offer an elevated creep-resistance for inhibiting the dislocations to climb over the $Al_{11}Ce_3$ lamella.

Along with the observations of the Al_3Sc coherent particles uniformly distributed in the Al_α matrix and the embellishment of the $Al_{11}Ce_3/Al_\alpha$ interface (see the sketch in Fig. 2(e)), we found that the creep resistance of Al-Ce alloy has been remarkably improved: the aged Al-12Ce-0.4Sc alloy can bear a much higher external stress than the Al-12Ce alloy in the tensile creep tests at 300 °C, see Fig. 4(a) showing the minimum strain rates $\dot{\varepsilon}$ vs. tensile stresses σ on a double-logarithmic plot. The values of apparent stress exponent, $n' = d(\log\dot{\varepsilon})/d(\log\sigma)$, have been marked on Fig. 4(a). To characterize the creep resistance by the stress threshold of dislocation creep σ_{th}, the existence of which is implied by the n' larger than the typical value for dislocation creep in pure Al ($n' < 5$ [37]), the relation $\dot{\varepsilon} = A(\sigma - \sigma_{th})^n \exp(-Q/RT)$ was used, where A is a dimensionless constant; n and Q are the true stress exponent and the activation energy for dislocation creep in Al_α respectively; R is the ideal gas constant and T is the temperature. Based on this relation, σ_{th} was estimated by extrapolating the linear regression line to $\dot{\varepsilon} = 0$ in the plot of $\dot{\varepsilon}^{1/n}$ vs. σ, and presented directly on Fig. 4(b). Note that the best linear fits were achieved when $n = 5$, implying the dislocation climb to be the main creep mechanism within the stress range explored.

With an age treatment at 400 °C for more than 3 h, the Al-12Ce-0.4Sc alloy displays a stress threshold of ~ 60 MPa (Fig. 4(b)), already higher than our elaborately designed Al alloys containing coarsening-resistant plate-like precipitates [17,18] and comparable to an outstanding Al-6Ni-0.4Sc alloy reported recently [23]. It should be noticed that their Al-6Ni matrix alloy overwhelms our Al-12Ce matrix alloy, see the comparison in Fig. 4(a). Therefore, with the same amount of Sc addition, the Al-12Ce-0.4Sc alloy catches up with the Al-6Ni-0.4Sc alloy in term of creep-resistance, indicating an optimization of the Sc effect in the Al-Ce system that has been discussed throughout the paper.

In summary, we alloyed the near-eutectic Al-12Ce alloy with Sc. A bidirectional influence between the elements Sc and Ce has been identified. On the one hand, the abundant Ce atoms interact with Sc during solidification and reduces the tendency of Sc partition between the liquid and solid phases. As a result, the microsegregation of Sc is largely suppressed, which ultimately results in a uniform distribution of Al_3Sc precipitates in the Al matrix upon aging. On the other hand, the interfacial precipitation of Al_3Sc layer or particles modifies the atomic structure of $Al_{11}Ce_3/Al_\alpha$ interface, which are believed to introduce additional lattice misfit strain inhibiting the dislocations to climb over the $Al_{11}Ce_3$ lamellae. With these two beneficial interactions, the creep resistance of the aged Al-12Ce-0.4Sc alloy is greatly improved, showing a high tensile stress threshold for dislocation climb of ~ 60 MPa at 300 °C.

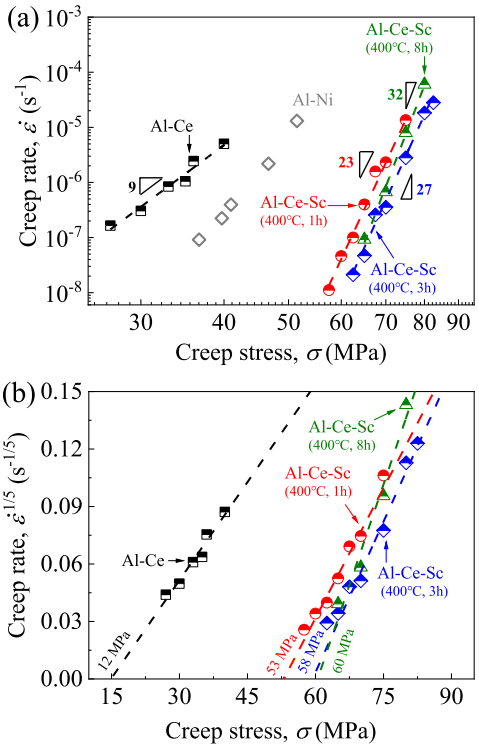

Fig. 4. Tensile creep properties. **(a)** Double-logarithmic plot of minimum creep rates vs. creep stresses at 300 °C for Al-12Ce and Al-12Ce-0.4Sc alloys. Data points of Al-6Ni alloy is taken from Ref.[23] **(b)** Linear plot of $\dot{\varepsilon}^{1/n}$ vs. σ with $n = 5$.

Declaration of Competing Interest

None.

Acknowlgedgments

This work was supported by the National Natural Science Foundation of China (51625103, 51790482, 51761135031, 52001249), the National Key Research and Development Program of China (2017YFB0702301), the Program of the Ministry of Education of China for Introducing Talents of Discipline to Universities (BP2018008) and the International Joint Laboratory for Micro/Nano Manufacturing and Measurement Technologies. P.Z. acknowledges the support from China Postdoctoral Science Foundation (2019M65359).

References

[1] M. Starink, S. Wang, Acta Mater 51 (17) (2003) 5131–5150.
[2] P. Zhang, J.J. Bian, C. Yang, J.Y. Zhang, G. Liu, J. Weiss, J. Sun, Materialia 7 (2019) 100416.
[3] R. Wang, S. Jiang, B. Chen, Z. Zhu, Journal of Materials Science & Technology 57 (2020) 78–84.
[4] L. Wu, Y. Li, X. Li, N. Ma, H. Wang, Journal of Materials Science & Technology 46 (2020) 44–49.
[5] K.E. Knipling, D.C. Dunand, D.N. Seidman, Zeitschrift für Metallkunde 97 (3) (2006) 246–265.
[6] A. Farkoosh, M. Pekguleryuz, Materials Science and Engineering: A 582 (2013) 248–256.
[7] F. Qian, S. Jin, G. Sha, Y. Li, Acta Mater 157 (2018) 114–125.
[8] Z.C. Sims, O.R. Rios, D. Weiss, P.E.A. Turchi, A. Perron, J.R.I. Lee, T.T. Li, J.A. Hammons, M. Bagge-Hansen, T.M. Willey, K. An, Y. Chen, A.H. King, S.K. McCall, Mater Horiz 4 (6) (2017) 1070–1078.
[9] D.R. Manca, A.Y. Churyumov, A.V. Pozdniakov, A.S. Prosviryakov, D.K. Ryabov, A.Y. Krokhin, V.A. Korolev, D.K. Daubarayte, Met. Mater. Int. 25 (3) (2018) 633–640.
[10] D. Weiss, J Mater Eng Perform 28 (4) (2019) 1903–1908.
[11] A. Plotkowski, O. Rios, N. Sridharan, Z. Sims, K. Unocic, R. Ott, R. Dehoff, S. Babu, Acta Mater 126 (2017) 507–519.
[12] A. Plotkowski, K. Sisco, S. Bahl, A. Shyam, Y. Yang, L. Allard, P. Nandwana, A.M. Rossy, R. Dehoff, Acta Mater 196 (2020) 595–608.
[13] D.S. Ng, D.C. Dunand, Materials Science and Engineering: A 786 (2020) 139398.
[14] Z.C. Sims, D. Weiss, S.K. McCall, M.A. McGuire, R.T. Ott, T. Geer, O. Rios, P.A.E. Turchi, JOM 68 (7) (2016) 1940–1947.
[15] Y. Liu, R.A. Michi, D.C. Dunand, Materials Science and Engineering: A 767 (2019) 138440.
[16] N.A. Belov, E.A. Naumova, D.G. Eskin, Materials Science and Engineering: A 271 (1–2) (1999) 134–142.
[17] Y.H. Gao, C. Yang, J.Y. Zhang, L.F. Cao, G. Liu, J. Sun, E. Ma, Materials Research Letters 7 (1) (2018) 18–25.
[18] Y.H. Gao, P.F. Guan, R. Su, H.W. Chen, C. Yang, C. He, L.F. Cao, H. Song, J.Y. Zhang, X. Zhang, G. Liu, J.F. Nie, J. Sun, E. Ma, Materials Research Letters 8 (12) (2020) 446–453.
[19] Q. Jia, F. Zhang, P. Rometsch, J. Li, J. Mata, M. Weyland, L. Bourgeois, M. Sui, X. Wu, Acta Mater 193 (2020) 239–251.
[20] D.N. Seidman, E.A. Marquis, D.C. Dunand, Acta Mater 50 (16) (2002) 4021–4035.
[21] E.A. Marquis, D.N. Seidman, Acta Mater 53 (15) (2005) 4259–4268.
[22] R.A. Michi, J.P. Toinin, A.R. Farkoosh, D.N. Seidman, D.C. Dunand, Acta Mater 181 (2019) 249–261.
[23] C. Suwanpreecha, J.P. Toinin, R. Michi, P. Pandee, D. Dunand, C. Limmaneevichitr, Acta Mater 164 (2019) 334–346.
[24] P. Pandey, S.K. Makineni, B. Gault, K. Chattopadhyay, Acta Mater 170 (2019) 205–217.
[25] W. Kasprzak, B.S. Amirkhiz, M. Niewczas, J Alloys Compd 595 (2014) 67–79.
[26] R. Mahmudi, P. Sepehrband, H. Ghasemi, Mater Lett 60 (21–22) (2006) 2606–2610.
[27] J. Robson, Acta Mater 52 (6) (2004) 1409–1421.
[28] K.E. Knipling, D.N. Seidman, D.C. Dunand, Acta Mater 59 (3) (2011) 943–954.
[29] S. Chen, S. Wang, H. Liang, J. Ma, G. Hu, Y. Dai, J. Yang, J. Zhang, Y. Yang, B. Sun, Acta Mater 188 (2020) 344–353.
[30] Q. Shi, Y. Huo, T. Berman, B. Ghaffari, M. Li, J. Allison, Scr Mater 190 (2021) 97–102.
[31] W. Kang, H. Li, S. Zhao, Y. Han, C. Yang, G. Ma, J Alloys Compd 704 (2017) 683–692.
[32] Z. Ahmad, Recent trends in processing and degradation of aluminium alloys, BoD–Books on Demand, 2011.
[33] K. Knipline, D. Dunand, Scr Mater 59 (4) (2008) 387–390.
[34] F. Czerwinski, B.S. Amirkhiz, Materials (Basel) 13 (20) (2020) 4549.
[35] E.A. Marquis, D.C. Dunand, Scr Mater 47 (8) (2002) 503–508.
[36] M.E. Krug, D.C. Dunand, Acta Mater 59 (13) (2011) 5125–5134.
[37] F.A. Mohamed, K.T. Park, E.J. Lavernia, Materials Science and Engineering: A 150 (1) (1992) 21–35.